Surface Growth and Oxidation of Soot Particles under Flame Conditions

Th. Schäfer[a], F. Mauß[b], H. Bockhorn[b], and F. Fetting[a]

[a] Institut für Chemische Technologie, Technische Hochschule Darmstadt, Petersenstraße 20, D-64387 Darmstadt

[b] Fachbereich Chemie, Universität Kaiserslautern, Erwin Schroedinger Straße Geb. 54, D-67663 Kaiserslautern

Z. Naturforsch. **50a**, 1009–1022 (1995); received August 29, 1995

Dedicated to Prof. Dr. Ewald Wicke on the occasion of his 80th birthday

Surface growth and oxidation of soot particles is investigated in premixed counter flow flames. Surface growth rates and soot oxidation rates can be evaluated from the measured appearance rates of soot and the calculated surface growth rates derived from the HACA-mechanism. The dependence of surface growth rates and soot oxidation rates on composition of the gas phase, temperature and "surface concentration" is discussed. A mechanism of soot oxidation accounting for the experimental findings is suggested.

1. Introduction

In recent years the basic knowledge of soot formation from hydrocarbon flames has been considerably improved by a number of experimental investigations and numerical modeling of laboratory flames and shock tube experiments. The most important results are summarized in several reviews, see e.g. [1–4], workshops and symposia, compare e.g. [5–7]. Particularly, the growth of soot particles in laminar premixed flames has been extensively studied, e.g. [8–17].

The formation of soot in premixed flames can be described in terms of particle inception, coagulation, surface growth and oxidation of soot particles. The formation of small soot particles is attributed to reactive coagulation of heavy polycyclic aromatic hydrocarbons (PAH) in the early stage of soot formation. While particle inception ceases after short time, the growth of soot particles due to coagulation and surface growth also occurs at later stages of soot formation. Particle inception and surface growth determine the total mass of soot, while particle coagulation only affects the size and the number density of the soot particles. The dynamics of particle coagulation are given by the laws of aerosol coagulation. It has been shown that the bulk of soot is formed by surface growth of the soot particles, see e.g. [9, 11, 13]. Particle inception contributes only to a small fraction of the final soot mass.

Reprint requests to Prof. H. Bockhorn.

From a phenomenological point of view soot formation in premixed flames follows a first order rate expression, compare e.g. [13]. The soot formation rate, which is commonly expressed in terms of soot volume fraction according to the equation

$$\frac{df_V}{dt} = k_{SG}(f_V^\infty - f_V), \tag{1}$$

is proportional to the difference of the final soot volume fraction f_V^∞ and the time dependent soot volume fraction f_V.

Integrating (1), assuming k_{SG} being independent of time, and substituting f_V leads to the equation

$$\frac{df_V}{dt} = k_{SG} f_V^\infty e^{-k_{SG}t}, \tag{2}$$

which gives an exponential decay of the soot formation rate with time.

The exponential decay is characterized by the coefficient k_{SG}, which depends on the maximum flame temperature with an apparent activation energy of 100–200 kJ/mol, see e.g. [11, 14]. The final soot volume fraction depends on pressure, temperature, composition of the feed and fuel structure. The temperature dependence is given by a bell shaped curve with a maximum final soot volume fraction at about 1700 K [14]. Up to a pressure of about 1 MPa the final soot volume fraction increases with the second power of pressure [11, 14].

It is meanwhile well accepted that surface growth of soot particles in hydrocarbon flames is dominated by

0932-0784 / 95 / 1100-1009 $ 06.00 © – Verlag der Zeitschrift für Naturforschung, D-72027 Tübingen

reactions of ethyne with the surface of the soot particles. A first approach of modeling surface growth was done by Harris and Weiner [8, 9], who supposed that the surface growth rate is proportional to the partial pressure of ethyne and the surface area of the particles. The further development of this model leads to the concept of active sites at the surface of the soot particles, compare e.g. [9, 10]. According to this, the surface growth rate is proportional to the number of active sites, which cover the surface and which are supposed not to be affected by coagulation and surface growth of the soot particles. The exponential decay of the surface growth rate is explained by a tempering process of the soot particles decreasing the number of active sites.

A new approach in modeling surface growth of soot particles, which allows for detailed chemical interpretation, has recently been introduced by Frenklach and Wang [18, 19]. The basic principles, which have been adopted meanwhile by a number of authors, see e.g. [20, 21], offer a key to the understanding of surface growth chemistry. The mechanism of surface growth is supposed to follow the planar growth of PAH according to a radicalic hydrogen-abstraction-hydrocarbon-addition (HACA) sequence.

Radicalic sites are formed by abstraction of hydrogen from arylic C-H bonds at the surface of the soot particles by hydrogen-, and to minor extent by hydroxyl radicals. The generated soot radicals are supposed to grow by the addition of ethyne. This is followed by a cyclisation step and by the cleavage of a C-H bond at the surface of the growing soot particle. The soot radicals involved in this sequence can be deactivated by molecular hydrogen and water molecules, thereby being prevented from growing.

Following this mechanism, the surface growth rate depends on the concentrations of the involved gaseous components (i.e. hydrogen- and hydroxyl radicals, molecular hydrogen, water molecules and ethyne) and, according to the rates of the various reaction steps under consideration, on temperature [18, 21]. The exponential decay of the surface growth rate is explained by the decay of hydrogen and hydroxyl radicals in the post flame zone of premixed sooting flames. In contrast to the models of Harris and Weiner [9] and Woods and Haynes [10] it is not necessary to introduce an unimolecular thermal deactivation of the soot particles.

Recent developments of mechanisms for soot formation include a kinetic description of soot oxidation by molecular oxygen and hydroxyl radicals, see e.g. [18, 22]. The experimental access to soot oxidation in premixed laminar sooting flames is difficult. Other laboratory flames are more suitable for the investigation of soot oxidation. Experiments have been carried out by several authors in coannular diffusion flames, see e.g. [23], two stage burners, compare e.g. [24, 25] and shock tubes [26, 27]. These experiments show that oxidation of soot particles under fuel rich conditions is mainly due to the oxidation by hydroxyl radicals [23–25]. With excess oxygen the oxidation occurs via molecular oxygen [27].

In recent experiments we have investigated surface growth and oxidation of soot in counterflow premixed twin flames [28]. Soot particles are formed in a premixed fuel rich ethyne-oxygen-flame counterflowing against a fuel lean flame of the same components or a mixture of oxygen in argon. The fuel lean flame contains a high level of hydroxyl radicals to oxidize the soot particles generated in the fuel rich flames. The experimental device allows a wide variation of the flame conditions, viz. temperature, particle size and number density, and composition of the gas phase surrounding the soot particles.

In the following, we will focus in particular on the oxidation of soot particles. Soot oxidation rates can be evaluated from the measured appearance rates of soot and the calculated surface growth rates derived from the HACA-mechanism. The dependence of the soot oxidation rates on temperature and composition of the gas phase will be discussed. Finally, a mechanism of soot oxidation, which can be used to interprete the experimental results, is suggested.

2. Experimental

The experimental setup is described in detail in [28]. A premixed sooting ethyne-oxygen flame, stabilized on a flat flame burner, is counterflowing against a premixed non sooting flame of the same fuel, stabilized on a second burner which contains excess oxygen and hydroxyl radicals to oxidize the soot particles generated in the sooting flame. Each of the two burners consists of a water cooled brass plate with about 800 holes with 1 mm diameter uniformly distributed over a circular area of 80 mm diameter at the center of each burner. The distance between the opposite burners amounts to 30 mm.

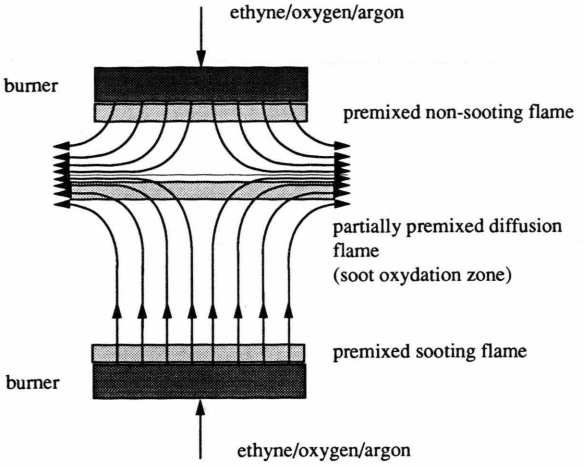

Fig. 1. Schematic diagram of counter flow premixed ethyne/oxygen flames, lower flame sooting, upper flame non-sooting.

The properties of the soot forming flame and the counterflowing non sooting flame can be easily controlled by the C/O-ratio of each feed and pressure. Figure 1 gives a schematic overview of the counterflowing flames.

The flames are investigated at low pressure (9 to 15 kPa) to obtain a better spacial resolution of the soot formation and oxidation zone. The burner system is equipped with all facilities for optical access and probe sampling. Soot volume fractions, mean particle radii and number densities are measured by means of laser light extinction and scattering. Gas samples of the flames are prepared with a quartz microprobe and analyzed with respect to the main stable gaseous species by mass spectrometry. Flame temperatures are obtained from thermal radiation of the soot particles appyling the Kurlbaum-method.

2.1 Extinction and Scattering Measurements

Soot volume fractions, soot particle radii and number densities are analysed by means of laser light extinction and scattering. For extinction measurements an argon-ion laser operating at a wavelength of 488 nm with a maximum power of 2 W has been used as light source. The optical path through the investigated flames was determined by shielding tubes, which are purged with nitrogen.

Two dimensional scattering measurements have been performed with a vertically polarized laser light sheet, which was obtained from expanding the laser beam with the aid of two cylindrical lenses. The scattered light was analysed with a CCD-camera (384 × 576 Pixel, 14 bit) with respect to its intensity, polarisation and wavelength. The scattering angle was 90°. The scattering area of 40 mm in radial and 27 mm in axial direction has been determined with a zoom objective in front of the camera. The scattering data are corrected with respect to thermal radiation of the flames. The experimental setup was calibrated with pure argon. The scattering cross section of argon is known [29].

The extinction and scattering data are evaluated assuming a complex refractive index of the soot particles of $1.57-0.56i$ [30], a spherical shape of the soot particles and a logarithmic normal size distribution with a standard deviation of 0.34 [11]. The latter assumption is an approximation for incipient soot formation and oxidation of soot particles where the shape of the particle size distribution changes. The small systematic errors arising from this assumption are discussed in [11, 12]. The soot particles in the investigated flames are small compared with the wavelength of the light, and hence the Rayleigh approximation for the evaluation of the scattering and extinction data can be used.

The extinction coefficients are evaluated with Lambert-Beer's law according to the equation

$$\ln(I/I_0) = -k_{ext}\, d, \tag{3}$$

where I_0 and I are the intensities of the incident and attenuated light, respectively, and d is the length of the optical path, which is defined by the distance of the shielding tubes (60 mm). k_{ext} represents the mean extinction coefficient along this distance.

The soot volume fraction f_V can be derived from the equation

$$f_V = \frac{k_{ext}}{\frac{6\pi}{\lambda}\,\mathrm{Im}\left(\frac{m^2-1}{m^2+2}\right)} = \frac{4}{3}\,\pi\, N_T \int_0^\infty r^3 f(r)\,\mathrm{d}r, \tag{4}$$

where m is the complex refractive index of the soot particles, λ the wavelength and k_{ext} the extinction coefficient as given by (3).

As shown in (4), the soot volume fraction is proportional to the number density of the soot particles N_T and to the third moment of the size distribution $f(r)$ of the particle radius r. Assuming a logarithmic normal size distribution with a median radius r_m and a

standard deviation σ, (4) takes the form [31]

$$f_V = \frac{4}{3}\pi N_T r_m^3 e^{4.5\sigma^2}. \tag{5}$$

Laser light sheet scattering gives a two dimensional picture of the scattering cross section Q_{vv} of the soot particles in the counterflow premixed twin flames, which depends on the local number density and median particle radius according to the equation

$$Q_{vv} = \frac{16\pi^4}{\lambda^4}\left|\frac{m^2-1}{m^2+2}\right|^2 r_m^6 e^{18\sigma^2} N_T. \tag{6}$$

The incident light is vertically polarized with respect to the scattering plane. Depolarization of the scattered radiation was negligible for the flame under investigation. This validates the Rayleigh approximation used for the evaluation of the scattering/extinction data. The scattering and extinction data are evaluated with respect to the median particle radius and number density by the combination of (5) and (6).

2.2 Gasphase Composition and Flame Temperature

Gas samples from the flames are prepared by means of a micro quartz tube which is installed vertically to the burner axis. The inner diameter at the top of the tube amounts to 150 µm. The tube could be adjusted at variable axial and radial positions in the burning chamber. The gas samples of the flames are analysed by means of a quadrupol mass spectrometer with respect to the composition of the main stable gaseous species.

The flame temperatures are derived from thermal radiation of the soot particles applying the Kurlbaum-method. The corresponding light intensity is detected by a photomultiplier at a wavelength of 488 nm. The dependence of the photomultiplier response on the black body temperature is known from the calibration of the experimental setup with a tungsten strip lamp. The temperature of the soot particles T is calculated by means of the equation

$$\frac{1}{T} = \frac{1}{T_s} + \frac{\lambda}{c_2}\ln(1-e^{-k_{ext}d}), \tag{7}$$

which can be derived from Wien's and Kirchhoff's laws of radiation [32]. T_s is the black body temperature of the soot particles and c_2 the second radiation constant according to Planck's law of black body radiation.

3. Results and Discussion

3.1 Gas Phase Composition

As an example from the measurements, the gas phase composition along the centerline of one of the investigated counter flow flames is given in Figure 2. The sooting flame for this particular experimental condition had a C/O-ratio of 1.25, whereas the non sooting flame had stoichiometric composition. Both ethyne/oxygen flames were diluted with argon (60% per volume), and the flow velocity for unburnt gas conditions amounted to 0.15 m s^{-1} for both flames. Pressure was 12 kPa.

In the sooting flame (lower flame) ethyne is converted predominantly to carbon monoxide and hydrogen. In the stoichiometric non sooting flame (upper flame) mainly water and carbon dioxide are formed. The stagnation region between the two flames forms a reaction zone where the products of the fuel rich sooting flame and the stoichiometric non sooting flame react within a kind of diffusion flame. Consequently, maxima of the CO- and H_2 mole fractions are located in the sooting flame, whereas those of CO_2 and H_2O are measured at about 25 mm height above the burner in the upper non sooting flame. The fuel of the non sooting flame is completely oxidized at 27 mm height above the burner. The increase near the stagnation plane of the counterflowing flames is due to diffusion of excess C_2H_2 from the sooting flame. The excess O_2 of the oxidizing flame vanishes at a short distance

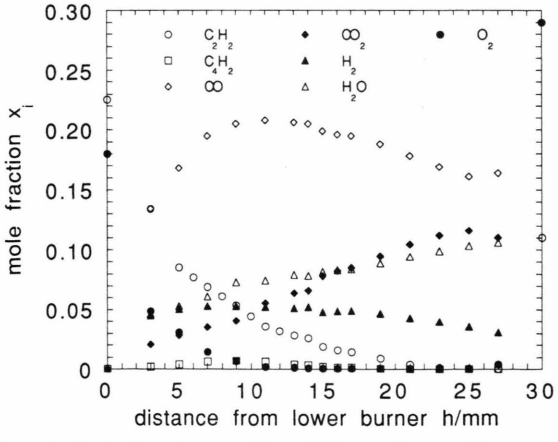

Fig. 2. Mole fraction profiles of the major stable components at the centre line for premixed counter flow flames; C/O-ratio lower flame: 1.25; C/O-ratio upper flame 0.40; pressure 12 kPa; unburnt gas velocity 0.15 ms^{-1} for both flames; feed of both flames contains 60% per volume argon.

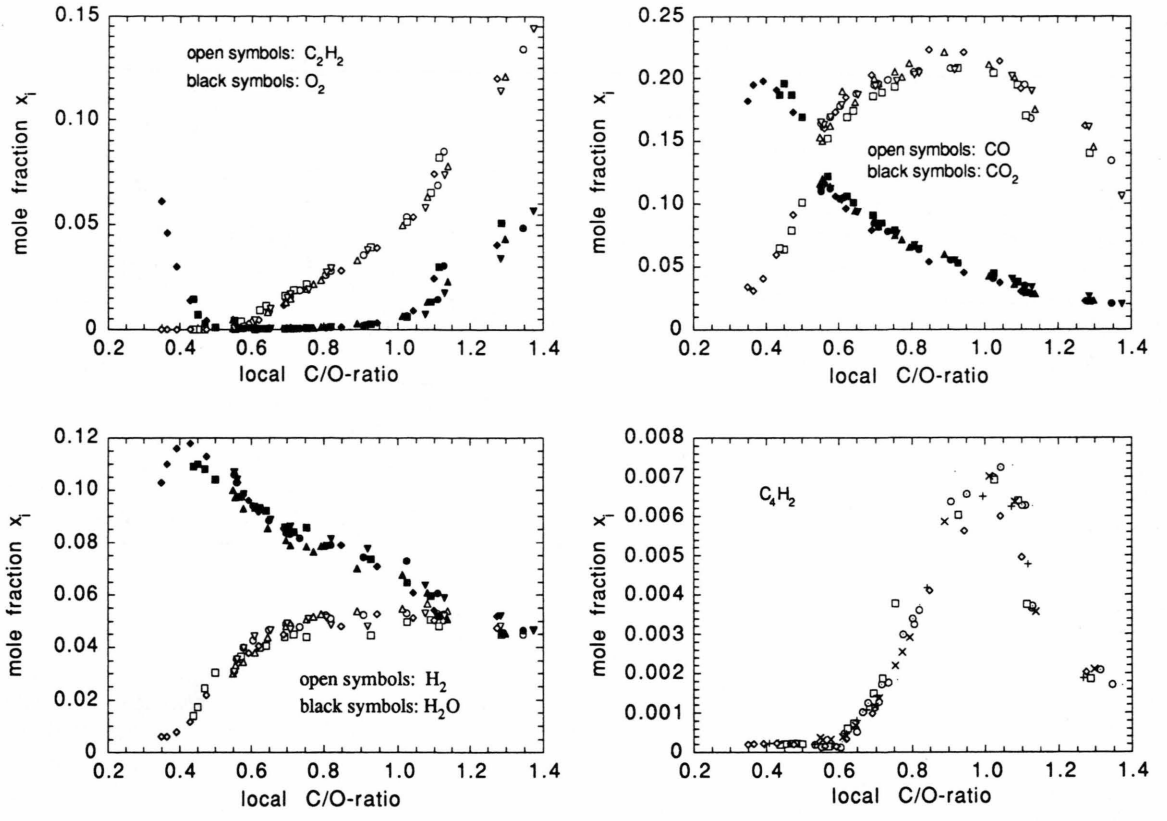

Fig. 3. Mole fractions of C_2H_2, O_2, CO, CO_2, H_2, H_2O, and C_4H_2 versus the local elementary composition for premixed counter flow flames; ▵: C/O-ratio lower flame 1.20; C/O-ratio upper flame 0.50; ×: C/O-ratio lower flame 1.20; C/O-ratio upper flame 0.35; ○: C/O-ratio lower flame 1.25; C/O-ratio upper flame 0.50; ○: C/O-ratio lower flame 1.25; C/O-ratio upper flame 0.45; □: C/O-ratio lower flame 1.25; C/O-ratio upper flame 0.40; +: C/O-ratio lower flame 1.25; C/O-ratio upper flame 0.35; ◇: C/O-ratio lower flame 1.25; C/O-ratio upper flame 0.30; ▽: C/O-ratio lower flame 1.30; C/O-ratio upper flame 0.50; ·: C/O-ratio lower flame 1.30; C/O-ratio upper flame 0.35; other conditions same as for flames in Figure 2.

beyond the reaction zone of that flame, caused by the reactions with CO and H_2. The mole fractions of H_2 and CO are considerably increased in the non sooting flame by diffusional transport from the sooting flame.

The local composition of the gas phase in the investigated flames depends on boundary conditions such as the C/O-ratio of the sooting and non sooting flames and pressure. When increasing e.g. the O_2 content in the oxidizing flame, an increase of the maximum mole fractions of CO_2 and H_2O and a shift of the position of the maxima towards the sooting flame is observed. Also, the mole fractions of C_2H_2, H_2, CO and also O_2 in the sooting flame are reduced. The latter result may be attributed to the temperature increase of the investigated flames when increasing the O_2 content of the oxidizing flame, which obviously accelerates the rate of the oxidation reactions in the sooting flame.

The counter flow flames may be regarded as a diffusion flame that is fed by the combustion products of a fuel rich and a fuel lean premixed flame. As a result of the fast chemical reactions occurring in this partially premixed diffusion flame the concentrations of the chemical species are adjusted to the local flame conditions, e.g. the local elementary mixture composition (C/O-ratio). Variations in the local elementary mixture composition of the two counter-flowing laminar flames may be attributed to variations of the gas phase composition, e.g. with increasing O_2 content of the oxidizing flame or with variation of other boundary conditions. Consequently, the concentrations of chemical species in the partially premixed diffusion flame should be similar, irrespective of the boundary conditions, when plotted versus the local elementary mixture composition (C/O-ratio). Figure 3 demonstrates

that the measured mole fractions of the major stable components for different flames with different boundary conditions coincide when plotting it versus the local C/O-ratio in the flames. The local C/O-ratio was obtained from the concentrations of all measured chemical species.

This behaviour is typical for laminar diffusion flames (flamelets) in the limit of fast chemical reactions. The structure of these flamelets in dependence on different boundary conditions can be uniquely described in terms of the local elementary mixture composition rather then in terms of geometric coordinates [33]. An additional "fine structure" overlayed over this structure is generated by the stretch of the flamelets due to velocity gradients and for the particular arrangement given in Fig. 1 (partially premixed flames) by the temperature of the premixed flames. For sooting flames a further parameter is the heat loss by thermal radiation of soot particles [34]. This fine structure has not been resolved in the present experiments.

3.2 Soot Volume Fraction, Number Densities and Mean Radii of the Soot Particles

Profiles of soot volume fractions, particle number densities and mean radii of soot particles along the center line of a number of flames are given in Figure 4. The experimental conditions for these flames are the same as for the flame in Figure 2. The C/O-ratio of the sooting flame is 1.25, and the C/O-ratio of the oxidising flame varies from 0.5 (stoichiometric) to 0.3 (fuel lean).

The soot volumen fractions increase approximately linearly between 5 and 10 mm height above the burner. The maximum soot volume fraction is attained shortly before the stagnation plane. Towards the stagnation plane of the counterflowing flames the soot volume fractions sharply decrease and the soot is completely oxidized. Increasing the O_2 content of the non sooting flames results in a decrease of the soot volume fraction gradients at low heights above the burner in the sooting flame, a gradually decrease of the maximum soot volume fractions and a shift of the maxima towards lower heights above the burner.

The gradients of the soot volume fraction profiles in the soot forming region of the sooting flames are determined by the net rates from surface growth and oxidation of the soot particles. The soot volume fraction gradients are proportional to the net appearance rates of soot (compare below). Increasing the O_2 con-

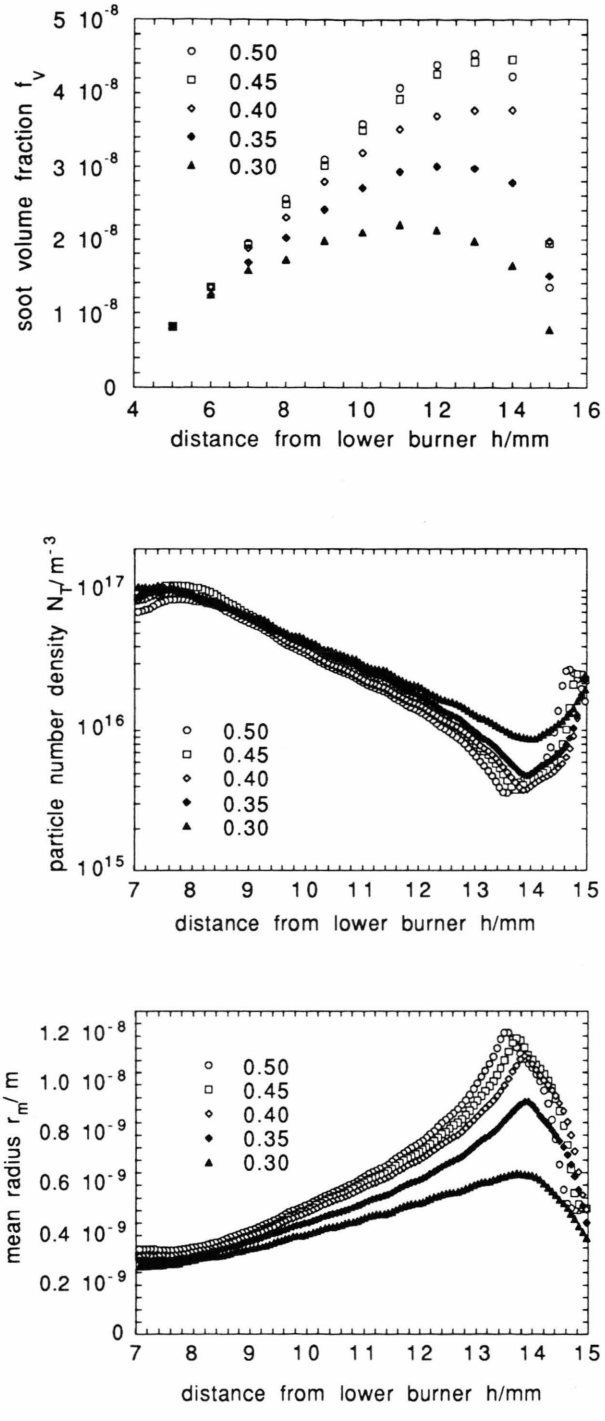

Fig. 4. Soot volume fractions, particle number densities and mean particle radii at the centre line for premixed counter flow flames; C/O-ratio lower flame 1.25; pressure 12 kPa; unburnt gas velocity 0.15 ms^{-1} for both flames; feed of both flames contains 60% per volume argon; numbers at the symbols mean C/O-ratio of the upper flame.

tent in the non sooting flame obviously accelerates the oxidation of the soot particles probably due to the increased diffusion of oxidizing species from the non sooting flame. Furthermore, the variations in soot volume fraction gradients may be attributed to the temperature increase or lower concentration of gaseous growth components (ethyne), which have been observed when increasing the O_2 content in the non sooting flame, compare Figure 3. The soot volume fractions at 5 mm height above the burner show negligible differences. This leads to the conclusion that surface growth of soot in the later phase of soot formation is affected by the O_2 content of the non sooting flame rather than particle inception in the early phase of soot formation.

Number densities and mean radii of the soot particles as evaluated from two-dimensional scattering and extinction measurements at the centerline of the same counterflow flames are also shown in Figure 4. The particle number densities increase at low heights above the burner and decrease rapidly towards higher heights above the lower burner due to coagulation of the soot particles. Consequently, the mean particle radii increase between 9 and 13 mm continuously.

Near the stagnation plane of the counter flow flames the number densities increase again, whereas the mean particle radii rapidly decrease. The maximum radii and minimum number densities are found for all flames at about 13.5 mm height above the burner, although the soot volume fractions decrease again between 10 and 13 mm. This indicates that coagulation of the soot particles continues under oxidizing conditions.

Near the stagnation plane of the flames the particle number densities strongly increase and the mean radii strongly decrease. The increase of particle number density is found to correlate with an 80% burnout of the soot particles. These results agree well with those of Neoh et al. [35] and may be explained with the internal burning of soot particles. OH-radicals are supposed to remove carbon atoms from the surface of the soot particles. While the oxidation of the soot particles proceeds, porous soot particles are formed. The penetration of less reactive O_2 into the pores of the soot particles then leads to the internal burning and finally to a break up of the porous soot particles into smaller units.

As evident from Fig. 4, the particle radii in the soot forming region of the lower flame decrease with increasing O_2 content in the oxidizing flame, whereas the number densities slightly increase. Therefore the specific surface area of the soot particles ("surface concentration") scarcely differs, especially at lower heights above the burner. The differences in the soot volume fractions in these flames can only be attributed to the change of the gas phase composition and/or temperature rather than to a change in the specific surface area.

The variation of the soot volume fractions with pressure and feed composition of the sooting flames is evident from Fig. 5, which shows the results of experiments with constant feed composition of the non sooting flame (C/O-ratio 0.3). The pressure varied from 9 kPa to 15 kPa and the C/O-ratio in the sooting flame was 1.20, 1.25 and 1.30, respectively. All other experimental conditions were identical to those in Figs. 2 to 4.

Changing the C/O-ratio of the sooting flames at constant pressure does not affect the shape of the profiles and the location of the maximum soot volume fractions. The steps in the increase of the C/O-ratio of the sooting flame result each in a 50% increase of the maximum soot volume fraction, whereas the shape of the curves with respect to the maximum soot volume fraction remains unchanged.

The strong variation of the soot volume fraction profiles with pressure is also obvious from Figure 5. Each pressure increase (9 kPa to 12 kPa and 15 kPa) results in a fourfold increase of the maximum soot volume fraction. The location of the maximum is

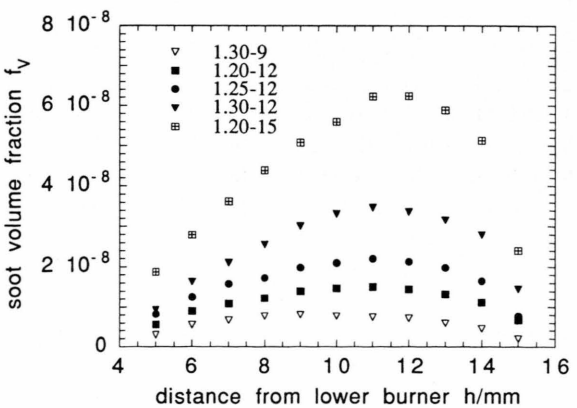

Fig. 5. Soot volume fractions at the centre line for premixed counter flow flames; C/O-ratio upper flame: 0.30; unburnt gas velocity 0.15 ms^{-1} for both flames; feed of both flames contains 60% per volume argon; numbers at the symbols mean C/O-ratio of the lower flame (first number) and pressure in kPa (second number).

shifted towards lower heights above the burner with decreasing pressure. This is probably caused by the decreasing diffusion rates of the gaseous species involved in the growth and oxidation reactions of the soot particles with increasing pressure.

The specific surface area of the soot particles strongly increases with pressure and the fuel content in the feed of the sooting flames. This correlates well with increasing appearance rates of soot. The differences in the soot volume fractions with varying pressure and feed composition of the sooting flames can be attributed to a change in the specific surface area and to the change of the gas phase composition and/or temperature. The appearance rate of soot (net rates from surface growth and oxidation of the soot particles) are obviously proportional to the soot volume fraction, i.e. the effective surface area accessible for surface growth and oxidation of the soot particles is presumably proportional to the soot volume fraction.

With respect to the soot volume fractions the partially premixed diffusion flames exhibit different behaviour than with respect to the gas phase composition. This is evident from Fig. 6, which gives the soot volume fractions plotted versus the local C/O-ratio of the counterflowing flames. The soot volume fraction profiles can not be uniquely correlated with the local C/O-ratio in the flames.

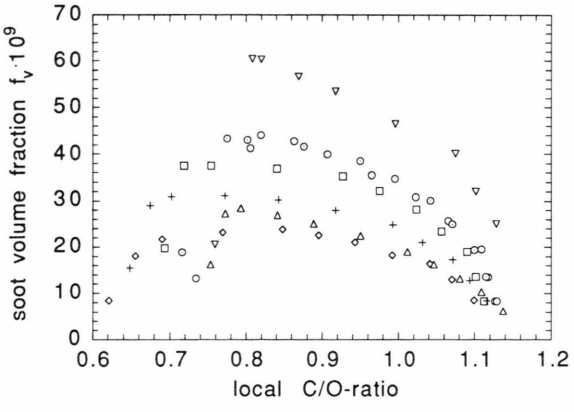

Fig. 6. Soot volume fractions versus the local elementary composition of premixed counter flow flames;
△: C/O-ratio lower flame 1.20; C/O-ratio upper flame 0.50;
○: C/O-ratio lower flame 1.25; C/O-ratio upper flame 0.50;
⊙: C/O-ratio lower flame 1.25; C/O-ratio upper flame 0.45;
□: C/O-ratio lower flame 1.25; C/O-ratio upper flame 0.40;
+: C/O-ratio lower flame 1.25; C/O-ratio upper flame 0.35;
◇: C/O-ratio lower flame 1.25; C/O-ratio upper flame 0.30;
▽: C/O-ratio lower flame 1.30; C/O-ratio upper flame 0.50;
other conditions same as for flames in Figure 2.

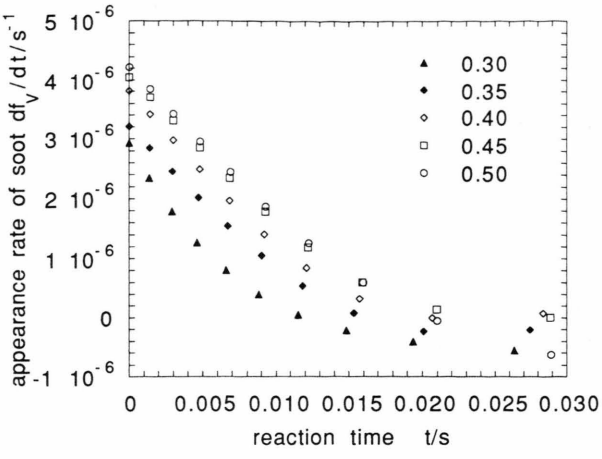

Fig. 7. Appearance rates of soot for the flames from Figure 4; numbers at the symbols indicate C/O-ratio of the upper flame.

4. Discussion

4.1 Net Appearance Rates of Soot

The net appearance rates of soot, which are proportional to the gradients of the soot volume fractions are exemplarly shown in Fig. 7 for counter flow flames, the sooting flame of which had a C/O-ratio of 1.25. The pressure amounted to 12 kPa and all other experimental conditions are as before. The O_2 content of the non sooting flame has been varied. The transformation of the height above the burner into time was done with the help of an approximation of the flow velocity considering variations in temperature and gas composition. The time scale is set to zero at 5 mm height above the burner.

The variation of the O_2 content of the upper non sooting flame results in a systematical decrease of the appearance rates of soot.

4.2 Surface Growth and Oxidation of the Soot Particles

The order of magnitude of the appearance rates of soot in the investigated counterflowing premixed twin flames at short reation times ($t < 10$ ms) agrees well with those from other investigations, e.g. [8–10]. Therefore, the specific rate coefficients for surface growth of the investigated flames at low heights above the burner (i.e. low reaction times) agree well with those in [8], when applying the corresponding model for surface growth.

Table 1. Comparison of calculated rates of oxidation of soot particles by O_2 with measured appearance rates of soot for some counter flow premixed flames; unburnt gas velocity 0.15 ms^{-1} for both flames; feed of both flames contains 60% per volume argon.

C/O-ratio lower flame	1.20	1.20	1.25	1.25	1.30	1.30	1.20	1.20
C/O-ratio upper flame	0.50	0.30	0.50	0.30	0.50	0.30	0.50	0.30
pressure/kPa	12	12	12	12	12	12	15	15
$\left(\frac{df_V}{dt}\right)_{calc}/s^{-1}$ at 10 mm	$-1.24\cdot10^{-7}$	$-1.77\cdot10^{-8}$	$-1.84\cdot10^{-7}$	$-3.22\cdot10^{-8}$	$-3.08\cdot10^{-7}$	$-7.20\cdot10^{-8}$	$-6.81\cdot10^{-7}$	$-4.44\cdot10^{-8}$
$\left(\frac{df_V}{dt}\right)_{exp}/s^{-1}$ at 10 mm	$1.12\cdot10^{-6}$	$1.93\cdot10^{-7}$	$1.87\cdot10^{-6}$	$3.90\cdot10^{-7}$	$2.63\cdot10^{-6}$	$8.83\cdot10^{-7}$	$4.20\cdot10^{-6}$	$1.58\cdot10^{-6}$
$\left(\frac{df_V}{dt}\right)_{calc}/s^{-1}$ at 13 mm	$-1.23\cdot10^{-8}$	$-3.29\cdot10^{-9}$	$-1.54\cdot10^{-8}$	$-3.34\cdot10^{-9}$	$-2.97\cdot10^{-8}$	$-8.05\cdot10^{-9}$	$-5.08\cdot10^{-8}$	$-2.68\cdot10^{-9}$
$\left(\frac{df_V}{dt}\right)_{exp}/s^{-1}$ at 13 mm	$1.15\cdot10^{-7}$	$-2.83\cdot10^{-7}$	$1.46\cdot10^{-7}$	$4.12\cdot10^{-7}$	$3.42\cdot10^{-7}$	$-6.14\cdot10^{-7}$	$9.11\cdot10^{-7}$	$-7.78\cdot10^{-7}$

The decrease of soot volume fractions at longer reaction times ($t > 10$ ms) indicates that at longer reaction times the oxidation rate exceeds the surface growth rate of the soot particles. The kinetics of soot oxidation by O_2 and OH-radicals are available from literature, see e.g. [1, 27, 24]. The oxidation rate of soot particles by molecular O_2 can be calculated employing a semiempirical rate expression given by Strickland-Constable and Nagle, which is valid for the oxidation of soot particles under O_2 rich conditions [1, 27]. The calculated oxidation rates df_V/dt(calc.) as evaluated from the equations in [27] are compared in Table 1 with the measured net appearance rates of soot df_V/dt(exp.) for some selected flames at 10 and 13 mm height above the lower burner.

The calculated oxidation rates amount to about 10% of the measured net appearance rates of soot, compare Table 1, indicating negligible contribution of soot oxidation by O_2 in that region of the flame. As shown exemplaryly for 13 mm height above the lower burner, the negative appearance rates of soot are considerably underestimated. Therefore, the oxidation of the soot particles in this region has to be attributed to other oxidizing species, probably OH-radicals. This result agrees well with those of several authors, e.g. [32], who found the oxidation of soot particles by O_2 being negligible in comparison with the oxidation by OH-radicals under slightly fuel rich conditions.

Surface growth and oxidation of the soot particles are mainly driven by C_2H_2 and OH, respectively, the mole fractions of which can be derived from the local elementary composition of the partially premixed flamelets, compare Figure 3. From this one would expect that the surface growth and oxidation rates of the soot particles also exhibit "flamelet" behaviour, i.e. that the appearance rates can be correlated with the local elementary composition of the partially premixed diffusion flames. Figure 8 demonstrates that the appearance rates of a variety of flames with different boundary conditions coincide when plotted versus the local C/O-ratio of the counterflowing flames. Similar results have been derived from the investigation of diffusion flames [36].

Application of the HACA-Mechanism to Surface Growth and Oxidation

According to the HACA-mechanism, surface growth occurs via several steps as shown in the following reaction schemes, compare e.g. [19, 37]:

H-abstraction, formation and deactivation of reactive soot radicals:

$$C_{x,i}H_y \overset{k_1}{\rightleftharpoons} C_{x,i}H^{\bullet}_{(y-1)} + H, \quad \text{(M1)}$$

$$C_{x,i}H_y + H \overset{k_2}{\rightleftharpoons} C_{x,i}H^{\bullet}_{(y-1)} + H_2, \quad \text{(M2)}$$

$$C_{x,i}H_y + OH \overset{k_3}{\rightleftharpoons} C_{x,i}H^{\bullet}_{(y-1)} + H_2O, \quad \text{(M3)}$$

Ethyne-addition and cyclisation:

$$C_{x,i}H^{\bullet}_{(y-1)} + C_2H_2 \overset{k_4}{\rightleftharpoons} C_{(x+2),i}H^{\bullet}_{(y-1)}, \quad \text{(M4)}$$

$$C_{(x+2),i}H^{\bullet}_{(y+1)} \overset{k_5}{\rightarrow} C_{(x+2),(i+1)}H_y + H, \quad \text{(M5)}$$

$$C_{(x+2),i}H^{\bullet}_{(y+1)} + C_2H_2 \overset{k_6}{\rightleftharpoons} C_{(x+4),i}H^{\bullet}_{(y+3)}, \quad \text{(M6)}$$

$$C_{(x+4),i}H^{\bullet}_{(y+3)} \overset{k_7}{\rightarrow} C_{(x+4),(i+1)}H^{\bullet}_{(y+2)} + H. \quad \text{(M7)}$$

Oxidation:

$$C_{x,i}H^{\bullet}_{(y-1)} + O_2 \overset{k_8}{\rightarrow} C_{(x-2),(i-1)}H^{\bullet}_{(y-1)} + 2CO, \quad \text{(M8)}$$

$$C_{x,i}H_y + OH \overset{k_9}{\rightarrow} C_{(x-2),(i-1)}H^{\bullet}_{(y-1)} + CHO + CH. \quad \text{(M9)}$$

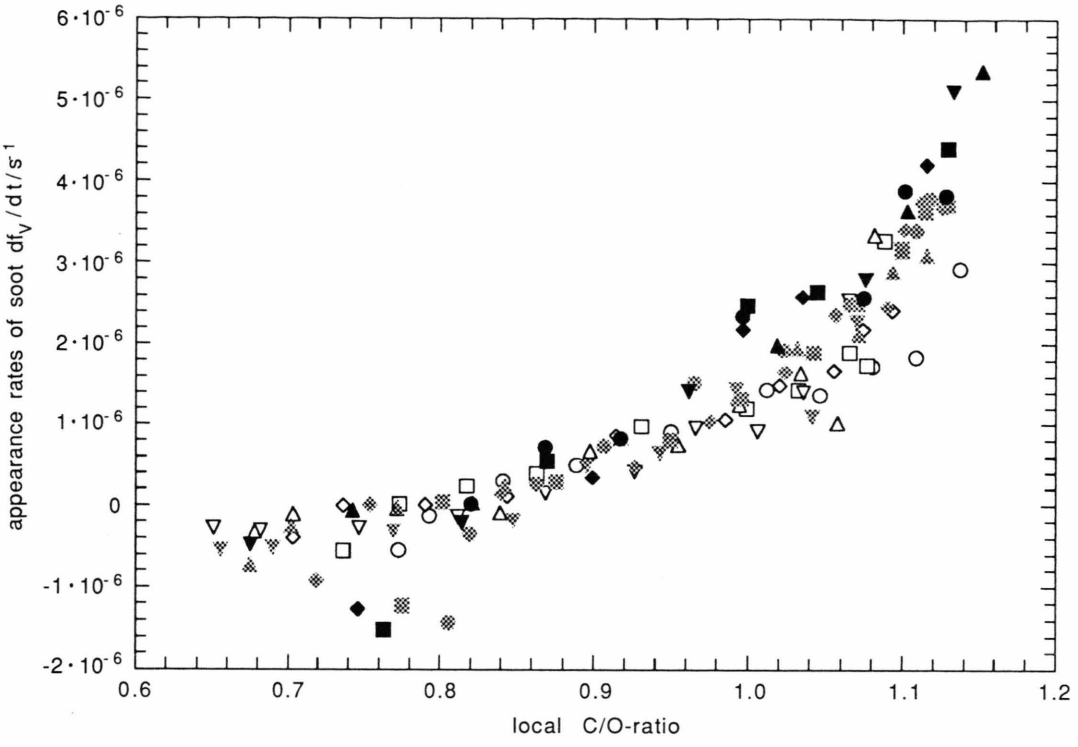

Fig. 8. Appearance rates of soot versus the local elementary composition for premixed counter flow flames; ○: C/O-ratio upper flame 0.50; □: C/O-ratio upper flame 0.45; ◇: C/O-ratio upper flame 0.40; △: C/O-ratio upper flame 0.35; ▽: C/O-ratio upper flame 0.30; *open symbols*: C/O-ratio upper flame 1.20; *grey symbols*: C/O-ratio upper flame 1.25; *black symbols*: C/O-ratio upper flame 1.30; other conditions same as for flames in Figure 2.

The indices x, y, and i in the formulae give the numbers of carbon atoms, hydrogen atoms and six membered aromatic rings within the growing soot particle. Active sites at the soot particle surface are formed by abstraction of H-atoms from arylic C-H bonds by H- and to minor extend by OH-radicals from the surrounding gas phase according to reactions (M2) and (M3).

The generated soot radicals can either add ethyne (M4) or are deactivated by the reversed reactions (M2) or (M3). Depending on the structure of the intermediate ethinyl-soot radical a further addition (M6) may follow. The reaction routes (M5) and (M7) provide cyclisation of the intermediate adducts to six membered carbon atom rings incorporated into the growing soot particles, which are stabilized be the cleavage of a C-H bond. Similar reasoning may be applied for the formation of five membered rings or other cyclic structures.

Thermal cleavage of aryl C-H bonds according to reaction (M1) contributes negligibly to the formation of soot radicals, whereas the reversed reaction (M1), viz. the deactivation of soot radicals by recombination with H-atoms, may be important under certain conditions. The reactions (M8) and (M9) account for the oxidation of the soot particles by molecular O_2 and OH-radicals. The reaction rates for the oxidation by O_2 from this model agree well with the rates from the rate expression given by Strickland-Constable and Nagle [1, 27].

For the specific experimental conditions of the flames under consideration the reaction scheme can be considerably simplified. The formation of soot radicals may be mainly attributed to the H-abstraction by H-atoms (M2), and deactivation is dominated by the reverse reaction (M2). The reactions (M6) and (M7) (addition of ethyne to the ethinyl-soot radical and consecutive cyclisation) contribute negligibly to the mass growth of the soot particles. Then, fragmentation (M4), cyclisation (M5) and ethyne-addition (M4) can be written in one comprehensive irreversible growth step:

$$C_{x,i}H^{\bullet}_{(y-1)} + C_2H_2 \xrightarrow{k_G} C^{\bullet}_{(x+2),(i+1)}H_y + H \quad \text{(MG)}$$

with

$$k_G = \frac{k_5 \cdot k_4}{k_{-4} + k_5}. \tag{8}$$

Assuming quasi-stationarity of the intermediate soot radicals, the dependence of the soot formation rate on the concentrations of the gaseous species contributing to growth, deactivation and oxidation is given by

$$\frac{df_V}{dt} \sim \frac{k_2[H](k_G[C_2H_2] - k_8[O_2])}{k_{-2}[H_2]} - k_9[OH]. \tag{9}$$

The relative rate of surface growth of the soot particles and oxidation by O_2 is given by the ratio $k_G[C_2H_2]/(k_8[O_2])$, that can be calculated using the experimentally measured mole fractions and temperature profiles as well as the rate coefficients from the described model. As shown in [28], at low heights above the burner these ratios agree well with the ratios of the net soot formation rates and the oxidation rates according to the kinetics of Strickland-Constable and Nagle. This indicates that oxidation of the soot particles by OH-radicals is neglibible at lower heights above the burner up to about 10 mm and validates the kinetics for soot oxidation by O_2 from [27].

Surface growth and oxidation of the soot particles by O_2 can be calculated by means of the proposed model, and the experimental results can be evaluated with respect to the oxidation of the soot particles by OH-radicals. In the maxima of the soot volume fraction profiles, the net soot formation rate df_V/dt for the corresponding heights above the burner is zero. Then, the rate coefficient k_G can be obtained from (9).

With $df_V/dt = 0$, from (9) follows

$$k_9 = \frac{k_2[H](k_G[C_2H_2] - k_8[O_2])}{[OH]k_{-2}[H_2]}. \tag{10}$$

The rate coefficients k_2, k_{-2}, k_G, and k_8 for the measured flame temperatures are adopted from the HACA-mechanism [22, 28]. The concentrations of the stable gaseous components are obtained from the experimental mole fraction profiles. The ratios of [H]/[OH] are estimated from the mole fractions of the water gas compounds assuming partial equilibrium of the reactions (E1) and (E2). The equilibrium constants of these reactions, $K_1(T)$ and $K_2(T)$ respectively, and their temperature dependence are known from literature [38].

$$CO + OH \overset{K_1(T)}{\rightleftharpoons} CO_2 + H, \tag{E1}$$

$$H_2 + OH \overset{K_2(T)}{\rightleftharpoons} H_2O + H. \tag{E2}$$

The rate coefficient k_9 for the location of maximum soot volume fractions according to (10) and the assumption of partial equilibrium for reactions (E1) and (E2) has been calculated for all flames under investigation. The temperature dependence of the rate coefficient is shown in Figure 9.

The filled and open symbols represent the results assuming partial equilibrium for reactions (E1) and (E2), respectively. The linear dependence of the rate coefficient k_9 on the reciprocal temperature indicates a negative apparent activation energy of -145 kJ/mole for the oxidation of the soot particles by OH-radicals. Additionally a linear pressure dependence of k_9 fits the data of the flames at different pressure. The negative activation energy of the oxidation reaction (M9) indicates that the oxidation of soot particles by OH radicals is a complex reaction comprising several

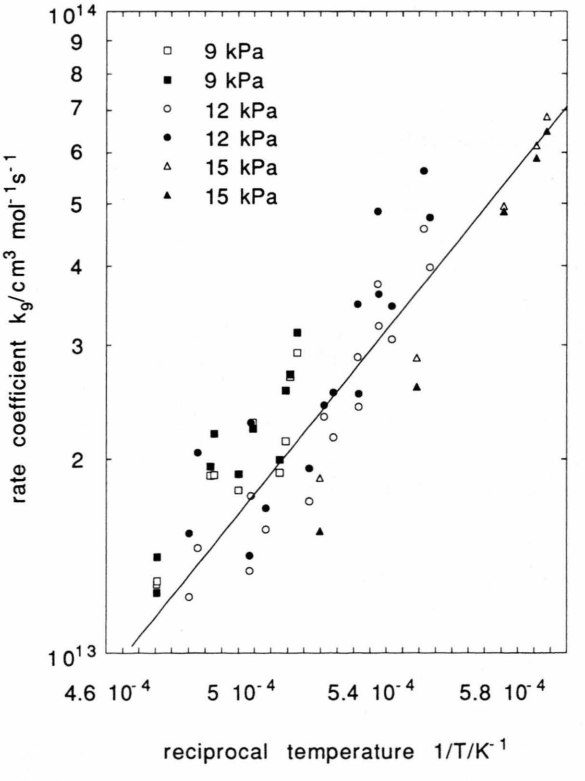

Fig. 9. Rate coefficient k_9 as defined by (10), plotted versus reciprocal temperature for the flames from Table 1; *open symbols*: partial equilibrium for reaction (E2); *black symbols*: partial equilibrium for reaction (E1).

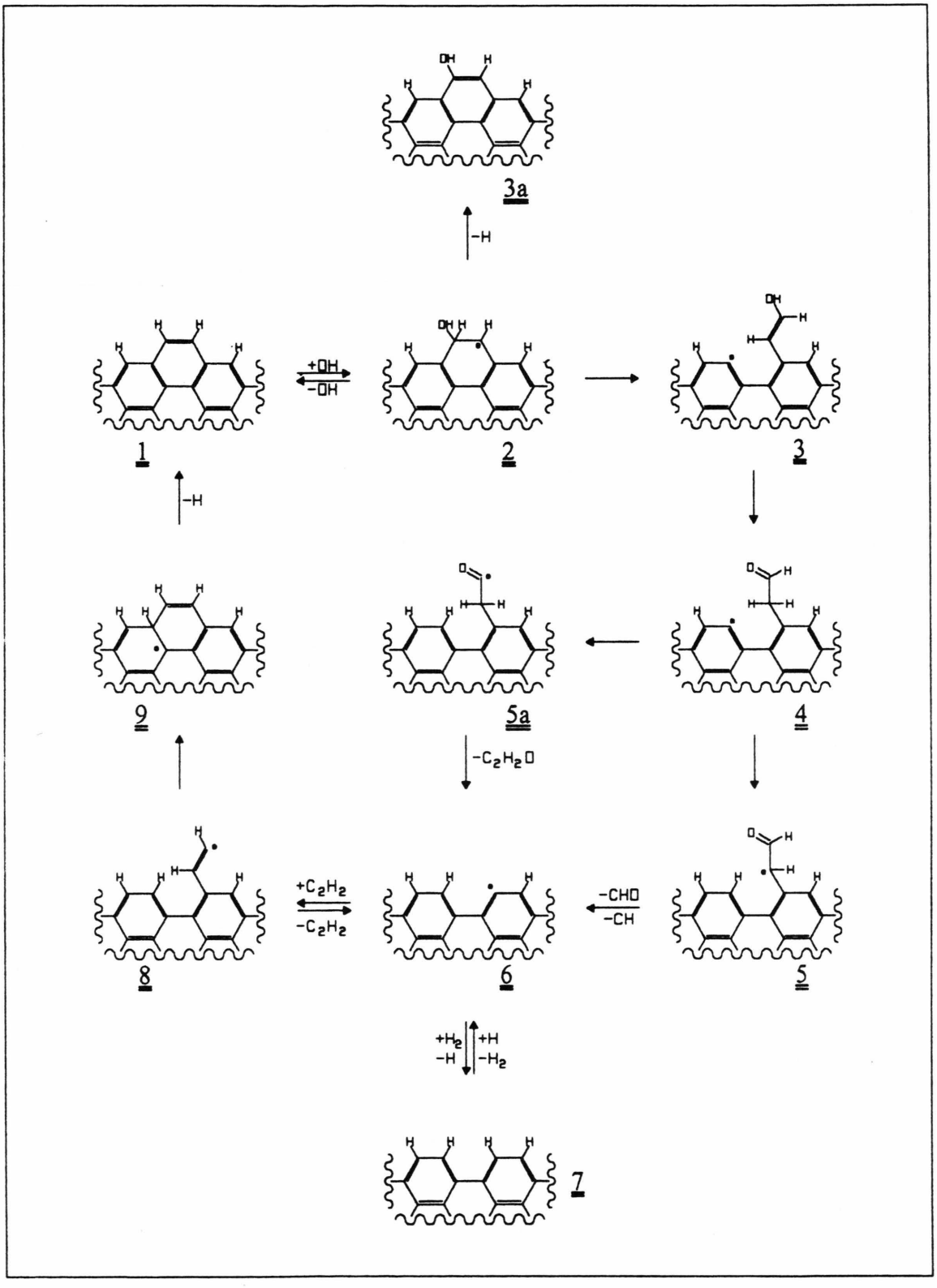

Fig. 10. Reaction scheme for surface growth and oxidation of soot particles under flame conditions.

steps. A possible mechanism of the oxidation of soot particles by OH-radicals, that accounts for this result, is proposed below.

The chemical mechanism of surface growth according to the HACA mechanism and the proposed mechanism of oxidation by OH-radicals is illustrated in Figure 10. The oxidation sequence starts with the reversible addition of OH-radicals ($\underline{1} \leftrightarrow \underline{2}$) to soot particles. The primary adduct decomposes via a sequence of reactions ($\underline{2} \rightarrow \ldots \rightarrow \underline{6}$). The oxidation products are CHO, CH and soot radicals, compare reaction (M9). The latter are stabilized by the addition of hydrogen ($\underline{6} \rightarrow \underline{7}$). The soot radicals formed within the oxidation sequence are also precursors for surface growth ($\underline{7} \rightarrow \underline{8}$). This can be considered in (10) by introducing an additional activation term.

The net reaction

$$C_{x,i}H_y + OH \overset{K_A(T)}{\rightleftharpoons} C_{x,i}H_yOH^{\cdot} \qquad \text{(M9)}$$

$$\rightarrow {}^{k_j} \rightarrow C_{(x-2),i-1)}H^{\bullet}_{(y-1)} + CHO + CH$$

depicts a simplified view of the oxidation mechanism. Assuming that equilibration of the addition step is faster then the following fragmentation reactions, the oxidation rate of the soot particles by OH-radicals r_{ox} can be expressed according to the equation

$$r_{ox} = k_j[C_{x,i}H_yOH^{\cdot}] = K_A k_j[C_{x,i}H_y][OH], \quad (11)$$

where K_A is the equilibrium constant of the initial OH-addition and k_j is the coefficient of the rate controlling step of the following reactions.

If the addition of OH-radicals to soot particles is exothermic, increasing temperature lowers K_A, and the equilibrium is shifted towards the educts of reaction (M9′). The experimental rate coefficient k_9 of the overall reaction (M9′) then decreases with increasing temperature if the k_j do not compensate this temperature dependence in the product $K_A k_j$. This simplified picture is consistent with the experimental findings given in Figure 9.

Negative activation energies of the overall oxidation reaction have been confirmed recently by investigations of Puri et al. [23], who investigated soot oxidation rates in coannular diffusion flames. They also found negligible contribution of O_2 to the oxidation of soot and a strong decrease of the reaction probability of soot oxidation by OH-radicals with increasing temperature.

Acknowledgement

This research was partially supported by the commission of the European Communities, the Swedish National Board for Technical Development (STU) and the Joint Research Committee of European car manufacturers (Fiat, Peugeot SA, Renault, Volkswagen und Volvo) within the IDEA and IDEA-EFFECT programs.

[1] B. S. Haynes and H. Gg. Wagner, Prog. Energy and Combust. Sci. **7,** 229 (1981).
[2] I. Glassman, Twenty-Second Symposium (International) on Combustion, p. 295, The Combustion Institute, Pittsburgh 1988.
[3] J. B. Howard, Twenty-Third Symposium (International) on Combustion, p. 1107, The Combustion Institute, Pittsburgh 1990.
[4] K. H. Homann, Twentieth Symposium (International) on Combustion, p. 857, The Combustion Institute, Pittsburgh 1984.
[5] D. C. Siegla and G. W. Smith (Eds.), Particulate Carbon: Formation during Combustion, Plenum Press, New York 1981.
[6] J. Lahaye and G. Prado (Eds.), Soot in Combustion Systems and its Toxic Properties, Plenum Press, New York 1983.
[7] H. Bockhorn (Ed.), Soot Formation in Combustion – Mechanisms and Models, Springer-Verlag, Berlin 1994.
[8] S. J. Harris and A. Weiner, Combust. Sci. and Tech. **32,** 267 (1983).
[9] S. J. Harris, Combust. Sci. and Tech. **72,** 67 (1990).
[10] I. T. Woods and B. S. Haynes, Combust. Flame **85,** 523 (1991).
[11] H. Bockorn, F. Fetting, A. Heddrich, and G. Wannemacher, Twentieth Symposium (International) on Combustion, p. 979, The Combustion Institute, Pittsburgh 1984.
[12] U. Wieschnowsky, H. Bockhorn, and F. Fetting, Twenty-Second Symposium (International) on Combustion, p. 343, The Combustion Institute, Pittsburgh 1988.
[13] B. S. Haynes and H. Gg. Wagner, Z. Phys. Chem. N.F. **133,** 201 (1982).
[14] H. Böhm, D. Hesse, H. Jander, B. Luers, J. Pietscher, H. Gg. Wagner, and M. Weiss, Twenty-Second Symposium (International) on Combustion, p. 403, The Combustion Institute, Pittsburgh 1988.
[15] H. Bockhorn and T. Schäfer, in: Soot Formation in Combustion – Mechanisms and Models, H. Bockhorn (Ed.), p. 250, Springer-Verlag, Berlin 1994.
[16] S. J. Harris and A. Weiner, Twenty-Second Symposium (International) on Combustion, p. 333, The Combustion Institute, Pittsburgh 1988.

[17] J. T. McKinnon and J. B. Howard, Twenty-Fourth Symposium (International) on Combustion, p. 333, The Combustion Institute, Pittsburgh 1992.
[18] M. Frenklach and H. Wang, Twenty-Third Symposium (International) on Combustion, p. 1559, The Combustion Institute, Pittsburgh 1990.
[19] M. Frenklach and H. Wang, in: Soot Formation in Combustion – Mechanisms and Models, H. Bockhorn (Ed.), p. 162, Springer-Verlag, Berlin 1994.
[20] M. B. Colket and R. J. Hall, in: Soot Formation in Combustion – Mechanisms and Models, H. Bockhorn (Ed.), p. 437, Springer-Verlag, Berlin 1994.
[21] F. Mauß, N. Peters, and H. Bockhorn, Proceedings of the Anglo-German Combustion Symposium, p. 470, The British Section of the Combustion Institute, Cambridge 1993.
[22] F. Mauß, Dissertation, RWTH Aachen (in preparation).
[23] R. Puri, R. J. Santoro, and K. C. Smyth, Combust. Flame **97,** 125 (1994).
[24] K. G. Neoh, J. B. Howard, and A. F. Sarofim, in: Particulate Carbon: Formation during Combustion, D. C. Siegla and G. W. Smith (Eds.), p. 261, Plenum Press, New York 1981.
[25] C. P. Fenimore and G. W. Jones, J. Phys. Chem. **71,** 593 (1967).
[26] P. Roth and O. Brandt, VDI Berichte Nr. 765, 67 (1989).
[27] C. Park and J. P. Appelton, Combust. Flame **20,** 369 (1973).
[28] T. Schäfer, Dissertation, TH Darmstadt (1994).
[29] R. R. Ruder and D. R. Bach, J. Opt. Soc. Amer. **58,** 1260 (1968).
[30] W. H. Dalzell and A. F. Sarofim, J. Heat Transfer **91,** 100 (1969).
[31] J. P. Hosemann, Chem.-Ing. Tech. **44,** 1015 (1972).
[32] U. Bonne and H. Gg. Wagner, Ber. Bunsenges. Phys. Chem. **69,** 35 (1965).
[33] N. Peters, Prog. Energy Combust. Sci. **10,** 319 (1984).
[34] K. M. Leung, R. P. Lindstedt, and W. P. Jones, Combust. Flame **87,** 289 (1991).
[35] K. G. Neoh, J. B. Howard, and A. F. Sarofim, Twentieth Symposium (International) on Combustion, p. 951, The Combustion Institute, Pittsburgh 1984.
[36] J. B. Moss, in: Soot Formation in Combustion – Mechanisms and Models, H. Bockhorn (Ed.), p. 544, Springer-Verlag, Berlin 1994.
[37] H. Bockhorn, F. Mauß and T. Schäfer, Combust. Flame **99,** 697 (1994).
[38] R. Stull and H. Prophet, JANAF Thermochemical Tables, Washington 1971.